METHODS 20, 341–361 (2000)
doi:10.1006/meth.1999.0927, available online at http://www.idealibrary.com on IDEAL®

Optical Spectroscopy in Studies of Antibody–Hapten Interactions

Sergey Y. Tetin*,[1] and Theodore L. Hazlett†

*Abbott Diagnostics Division, Abbott Laboratories, Abbott Park, Illinois 60064; and
†Laboratory for Fluorescence Dynamics, Department of Physics, University of Illinois at Urbana-Champaign, Urbana, Illinois 61801

This article describes the use of optical spectroscopy in studying antibody–hapten interactions and in determining the equilibrium binding constants. Along with equilibrium binding data, spectroscopic tools often deliver structural information on binding-induced conformational changes of antibodies (or haptens). Structural implications of results from example antibody–hapten systems are included. Fluorescence spectroscopy has been particularly useful in the area of ligand binding, and thus steady-state fluorescence quenching and fluorescence polarization are the primary techniques under discussion. A brief description of fluorescence correlation spectroscopy is also provided. Absorption techniques, including circular dichroism, are mentioned to a lesser extent. A basic description of the mathematical models involved in the analysis of binding equilibria is provided along with references to more complete works. Simulated and experimental data are used to illustrate the various experimental protocols and the appropriate analytical methods. Typical sources of errors and experimental precautions are indicated throughout the general discussion. © 2000 Academic Press

The ability of the immune system to recognize and eliminate foreign material has been under intense investigation for decades. The early research aims of this field focused on the capacity of the immune system to recognize a surprisingly wide variety of antigens and subsequently construct specific antigen-directed antibodies. Biomolecular recognition, of course, is not the sole property of the immune system but is found in virtually every cellular process. As cellular functions evolved, the cell required an increasingly complex mechanism for recognition. In the immune system, this general cellular feature was directed toward the separation of self from nonself agents and the elimination of nonself material.

Clearly, understanding functional interactions among proteins, carbohydrates, lipids, DNA, RNA, substrates, and cofactors is a vital and critical research endeavor in biology and biochemistry. The key process for most protein functions is the specific recognition of an appropriate ligand (substrate, allosteric regulator, transported metabolite, hapten, drug, or other molecules) or another protein (other subunits in multisubunit proteins, receptor, the next protein in cascade mechanisms, forensic protein). These processes result in biological specificity. The strength of the interaction of reacting molecules is characterized by an equilibrium binding constant expressing biological affinity.

The ability of the immune system to form antibodies against foreign antigens makes antibodies extremely useful tools in biochemistry. Detection of known antigens, such as viral antigens, bacterial antigens, and drug presence, is commonly used in biomedical practice by means of the immunoassays. Additionally, antibodies can serve as model systems for probing the details of well-defined ligand–protein or protein–protein associations.

Antibodies and receptor proteins of the immune system demonstrate the range of typical biologically relevant specificities and affinities. The structure–function relationships in several antibody–antigen systems have been intensively studied for the past three decades (recently reviewed (1)). Several antibody–hapten complexes have been crystallized, and their three-dimensional structures can be found in the Protein Structure Data Bank. It is generally accepted that the antibody binding site accommodates a single hapten

[1] To whom correspondence should be addressed at D-4H4, AP-20, Abbott Laboratories, 100 Abbott Park Road, Abbott Park, IL 60064-6016. Fax: (847) 938-2510. E-mail: sergey.tetin@abbott.com.

1046-2023/00 $35.00

molecule and that the binding sites in immunoglobulins do not interact in binding of haptens in solution. This understanding allows us to restrict the discussion here to the simple binding model (identical, noninteracting binding sites). However, the researcher should not overlook other binding mechanisms. It is possible that two or more hapten molecules can be simultaneously accommodated at the antibody binding site or for the hapten molecule to bind to the antibody outside the typical binding site in a nonspecific manner. Furthermore, occasional speculation on interactions between binding sites of the same antibody after hapten association is often discussed, despite the absence of experimental support. Generally speaking, properly determining stoichiometry, carefully performing experimental work, and minimizing data transformation during analysis will provide the bases for application of an appropriate binding model.

We will use the term ligand here for organic molecules (molecular mass 100–1000 Da) that are significantly smaller than antibody molecules (150,000 Da for IgG). The ligand usually is unable to induce an immune response alone but may act as an immunogenic epitope when attached to a macromolecular carrier. Subsequently, the ligand will be recognized by induced antibodies and will act as an antigenic determinant (or antigenic epitope). The immunology literature identifies such ligands as haptens (2). Ligand is a more common term in protein studies, but it also has been used often in immunochemistry. Therefore, in our further discussions, we use ligand and hapten as equivalent terms.

The overall aim of this article is to introduce the reader to the use of optical spectroscopy in the study of antibody–ligand interactions and in the determination of the equilibrium binding constant. Various methodologies in fluorescence spectroscopy have been particularly useful in the area of ligand binding and are the primary techniques under discussion. Absorption techniques, including circular dichroism, are mentioned but to a lesser extent. Because the experimental design goes hand-in-hand with a firm basic understanding of the processes involved, a section is devoted to the general equilibrium model and its mathematical description. We hope the following discussions, although focused on simple single-site binding, will be of use to students and researchers in the field. If the reader desires more elaborate and complete work on ligand binding, the literature contains a variety of excellent work (3–10).

THEORETICAL CONSIDERATIONS

Ligand Binding

A simple binding equilibrium between protein [P] and ligand [L] is described by the reaction

$$[\mathrm{LP}] \rightleftharpoons [\mathrm{L}] + [\mathrm{P}], \qquad [1]$$

where the dynamic equilibrium between the protein–ligand complex [LP] and the free species is related. The equilibrium constants, the dissociation constant K_d, and the association constant K_a, for this equilibrium are described by the relationship

$$K_d = \frac{1}{K_a} = \frac{[\mathrm{L}][\mathrm{P}]}{[\mathrm{LP}]}. \qquad [2]$$

For the simple equilibrium described in Eq. [2], the dissociation constant will have units of concentration and the association constant will be in reciprocal concentration units. For this reason, it is often more natural to think in terms of dissociation constants, which, in these cases, also define the concentration at which 50% ligand is bound.

The equilibrium constants are directly related to the binding free energy, ΔG, the enthalpy, ΔH, and the entropy, ΔS, by the equation

$$\Delta G = -RT \ln(K_a) = \Delta H - T\Delta S, \qquad [3]$$

where R is the gas constant and T is the temperature. The enthalpic and entropic contributions to the binding free energy can be evaluated by measuring ΔG as a function of temperature, which has a predominant effect on the $T\Delta S$ term. The hydrophobic and electrostatic contributions to the binding reaction tend to favor entropic effects and can be explored by following the ΔG as a function of the solution ionic strength. The presence of electrolytes should weaken, via charge screening, electrostatic forces and help in estimating the contributions of salt bridges to the binding energies. Piecing together the forces involved in the binding reaction can help to define the responsible contacts, but this is not always the experimental aim. A great deal of research is directed solely toward the detection of ligand binding and the subsequent characterization of the dissociation constant. Rapid drug screening in the pharmaceutical industry is a good example of the detection of binding between potential drugs and target molecules being a primary research focus. In either case, determination of the equilibrium constant is often a critical first step.

Equilibrium Binding

Experiments designed to measure the binding between ligand and protein must have an observable parameter that is proportional to the fraction of binding sites filled, F_b. In our simple case above, with one binding site per protein (Eq. [1]), F_b will range from 0 to 1 and will be defined as

$$F_b = \frac{[LP]}{[P] + [LP]} = \frac{[LP]}{[P_t]}, \quad [4]$$

where $[P_t]$ is the total protein concentration. As mentioned in the introduction, antibody binding sites are equivalent and noninteracting, qualities that permit us to treat each site as a distinct element. Equation [4] can be modified to accommodate IgG antibody and hapten binding by substituting the free protein concentration, [P], with the concentration of available sites, [S], and substituting [LS] for [LP] as the ligand–site complex:

$$F_b = \frac{[LS]}{[S] + [LS]} = \frac{[LS]}{[S_t]}. \quad [5]$$

Our experimental goal here is to accurately determine the K_d of a particular ligand and IgG pair. The fraction of sites bound, F_b, and the total solution concentrations of sites, $[S_t]$, and ligand, $[L_t]$, will be known quantities. The relationship between the fraction of bound complex with S_t, L_t, and K_d can be derived from Eqs. [2] and [5] and is given by

$$F_b = \frac{K_d + S_t + L_t - (K_d^2 + 2K_dS_t + 2K_dL_t + S_t^2 - 2S_tL_t + L_t^2)^{1/2}}{2S_t}. \quad [6]$$

In conjunction with Eq. [9] (below), Eq. [6] can be used to fit experimental data and resolve K_d by successive approximations (11).

The classic description of the ligand binding problem is Adair's equation (12), given below for n binding sites,

$$v = \frac{\sum_{i=1}^{n} i(\prod_{i=1}^{n} K_i)[L]^i}{1 + \sum_{i=1}^{n} (\prod_{i=1}^{n} K_i)[L]^i}, \quad [7]$$

where v is the binding in moles of ligand bound per mole of protein, L is the concentration of free ligand, and K_i are the Adair constants, which is related, but not identical, to the individual site dissociation constants. The Adair constants are also termed the macroscopic equilibrium constants and represent the affinity of a ligand for the nth binding site in a sequence of bindings. These constants are not identical to the equilibrium constants for the individual sites, the microscopic equilibrium constants, because of statistical effects (see (13) and references within for a more detailed discussion of micro- and macroequilibrium constants). In our discussions, we are interested in the microequilibrium constants that measure the affinity of the individual sites and relate to the free energy of binding (Eq. [3]). Obviously, for single-site proteins the macro- and microequilibrium constants are identical. In the case of distinguishable noninteracting sites, the microequilibrium constants are measured directly, and Eq. [7] can be simplified (14) to

$$v = \sum_i \frac{s_i[L]}{K_{d_i} + [L]}, \quad [8]$$

where i is the number of site populations, K_{d_i} is the common dissociation constant (the microequilibrium constant) for the ith population, and s_i is the number of sites within the ith population. By introduction of the F_b term and adaption for IgG, which contains two equal affinity sites ($i = 1$ and $s_i = 2$), Eq. [8] reduces to

$$F_b = \frac{v}{2} = \frac{[L]}{K_d + [L]}. \quad [9]$$

Equation [9] can also be derived from Eqs. [2] and [5] and is the standard equation used to fit antibody binding data. Binding curves for IgG–hapten pairs having dissociation constants of 0.1, 1, and 10 nM are simulated in Fig. 1. In the traditional ligand binding experiment, the number of binding sites (or protein concentration) is kept constant while the concentration of ligand is progressively increased. The fraction of bound sites, F_b, should be plotted as a function of free ligand concentration. A logarithmic scale is recommended for the abscissa to accommodate the wide range of ligand concentrations required to span the complete binding profile. The data are then fit to Eq. [9] through the use of a regression procedure, such as the commonly applied least-squares procedures or maximum likelihood method (7), from which the K_d is determined.

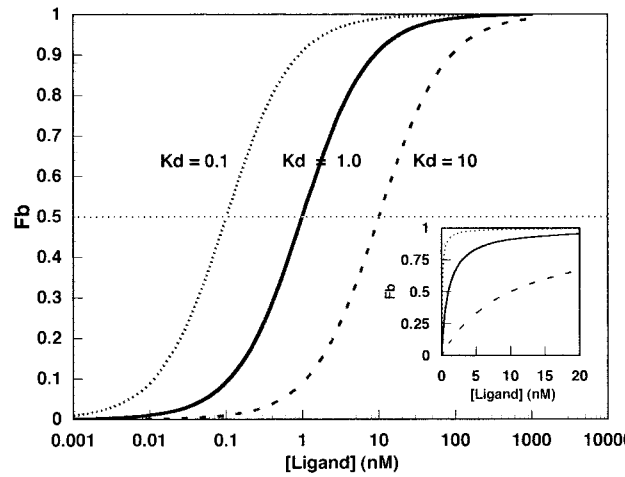

FIG. 1. Equilibrium binding curves for site–ligand dissociation constants of 0.1 nM (dotted line), 1.0 nM (solid line), and 10 nM (dashed line). Inset: Plot contains the identical curves plotted on a reduced linear scale.

The total ligand concentration is used routinely as an estimate of the free ligand concentration and is used in the binding analyses. This assumption is acceptable as long as the concentration of bound ligand remains small relative to the total ligand. If, however, the fraction of ligand bound is significant, then one must find a manner to determine the amount of free ligand present. In experiments in which the fraction bound is determined directly, one can immediately and simply calculate the free ligand concentration by $L = L_t - (F_b \times S_t)$. In cases where F_b cannot be directly calculated, one can use the aforementioned stepwise procedure entailing the calculation of an *apparent* K_d, using Eq. [9] with the total ligand concentration, from which an estimation of the *apparent* free ligand concentration is made through application of Eq. [6], again to be applied in calculating a new apparent K_d. Several iterations between Eqs. [9] and [6] should lead to accurate values for K_d and the free ligand concentrations. When the precision of the data is poor or the fraction of ligand bound is large, this iterative procedure will not properly converge. There are many more robust procedures given in the literature (7, 9, 15, 16), but for a simple binding problem the iterative method can suffice. As a general rule, if the ratio of sites to K_d is below 0.1, then the total ligand should be a close approximation of the free ligand concentration.

The effect of using total ligand for free ligand under inappropriate conditions is illustrated in Fig. 2, where the curves represent increasing ligand/K_d ratios. As a consequence of the increasing ligand/K_d ratio, the apparent K_d, often taken as the 50% bound point, shifts to higher values as the stoichiometric limit is approached.

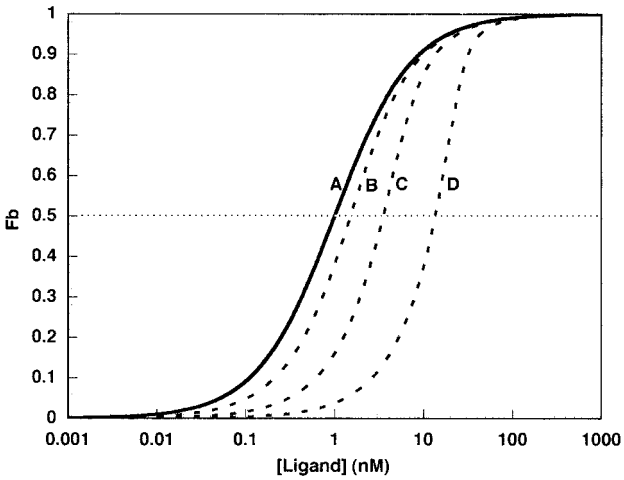

FIG. 2. The effect of stoichiometric binding conditions on the binding isotherm. Curves are plotted as the fraction sites bound versus the total ligand concentration. The solid line (A) is the expected curve, under conditions where $[\text{Ligand}]_{total} \approx [\text{Ligand}]_{free}$, for a dissociation constant of 1 nM. The dashed lines illustrate the resulting curves when the concentration of sites is increased to 1 (B), 5 (C), and 25 (D) times the K_d.

A prudent investigator will verify the validity of a binding profile experimentally by repeating the titration at a lower concentration of binding sites. The determined K_d should remain unchanged.

It is often preferable to fit raw data directly rather than to convert data to estimates of F_b. If the observable parameter is linearly related to the fraction bound, then Eq. [9] can be applied but it must be multiplied by a scaling factor (m), to match the parameter's range, and a constant (c) must be added to account for the observed parameter having a nonzero value for the unbound state:

$$F_b = \frac{m[\mathrm{L}]}{K_d + [\mathrm{L}]} + c. \qquad [10]$$

The scaling factor and constant are usually fit as free parameters in the data analysis. Examples of binding experiments are given later in this article, along with discussion on the appropriate calculations for F_b.

The binding experiments described so far have followed protocols that hold the concentration of sites constant while the ligand concentration has been varied. One may also carry out the opposite, but equivalent, experiment in which the ligand is held constant and the site's concentration is changed. The binding plots from the two experiments should follow Eq. [9] and be essentially identical, as long as there is a single dissociation constant. In monoclonal IgG preparations it is reasonable to assume a single K_d. Polyclonal IgG, on the other hand, contains a population of IgG species with a distribution of binding constants and is thus more complicated. The shapes of the resulting binding profiles will depend on the number of dissociation constants present, the range of dissociation constants, and the experimental protocol used. For the condition when the concentration of sites, representing a number of K_d values, is held constant, the presence of additional dissociation constants increases the span of the binding profile. When there is a mixture of two antibodies with a 100-fold difference in K_d values, one can easily see the impact of each equilibrium constant on the complete binding profile (Fig. 3A). In contrast, on the binding plot for an experiment in which the ligand is held constant and the IgG mixture is added, one observes a binding curve possessing a normal profile that can be well fitted to a single K_d. In the extreme case presented in Fig. 3B, the fraction of bound ligand is almost exclusively due to ligand association with the high-affinity site. The shift in the K_d is a result of the fact that 50% of the added antibody, the weak binding portion, participates little in the actual binding but continues to add to the total antibody concentration. In situations in which the affinities are closer, the tight affinity site remains the primary ligand binding site,

and identifying the presence of multiple K_d values is exceedingly difficult using this protocol.

Equilibrium Dilution

A second, less common, experimental procedure for measuring a binding profile is to prepare an equimolar solution of ligand and binding sites at saturating concentrations and proceed to dilute the mixture (8). As the concentration of ligand and protein fall, the protein and ligand will dissociate. Given the definition of K_d and that the concentrations of the ligand and binding sites are equal, the K_d becomes

$$K_d = \frac{[S]^2}{[LS]}, \qquad [11]$$

and the relationship between the total sites, F_b, and K_d is

$$F_b = \frac{K_d + 8S_t - (K_d^2 + 16S_tK_d)^{1/2}}{8S_t}. \qquad [12]$$

A sample binding plot is given in Fig. 4, where F_b is plotted as a function of the sum of the concentrations of ligand and sites which places the 0.5 fraction bound at the K_d.

The curves in Fig. 4 look similar to the standard binding curves in Fig. 1 and are plotted in a manner similar to the standard plots with the dissociation constants at $0.5F_b$. The dissociation constants are the same in both Figs. 1 and 4, but one should note that the span of the dilution binding curve ($0.1F_b$ to $0.9F_b$) is 2.86 log units and not 1.90 log units as in the standard binding profile.

Stoichiometric Binding

In experiments designed to determine an equilibrium constant, stoichiometric binding conditions are to be avoided, but in experiments designed to determine the number of sites per protein, stoichiometric conditions *are required*. An illustration of how the number of ligand binding sites per protein is determined is given in Fig. 5. In this example, the ligand is held constant, at concentrations well above the suspected dissociation constant, and protein is used as the titrant. The fraction of ligand bound is then plotted as a function of the moles of protein added per mole of ligand. Two dashed lines are drawn from the plot: (i) the stoichiometry line that is extrapolated from low protein additions where the change in F_b is linear with addition of binding sites, and (ii) the saturation line drawn at high protein concentrations when most ligand is bound and further addition of protein has little effect on F_b. The intersection of these two lines, indicated by the dotted drop line, should mark the number of moles of ligand bound per mole of protein, the binding stoichiometry. It should be noted in Fig. 5 that the saturation line is not at 1.0, as it should be. With

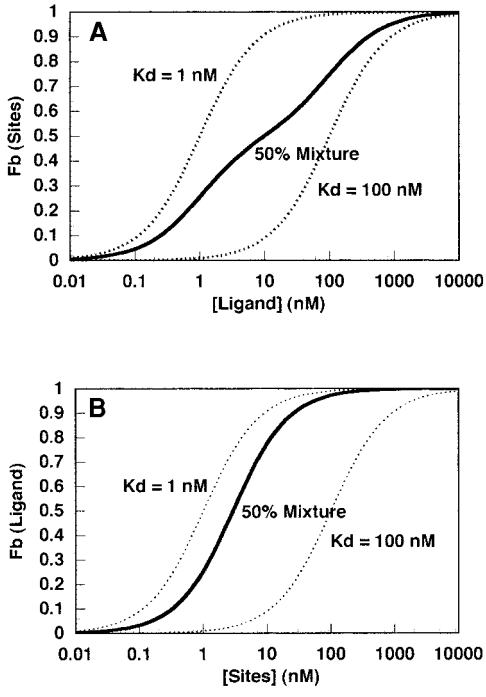

FIG. 3. Simulated binding curves for a two-component mixture containing 0.5 mol fraction for each of two IgG species having dissociation constants for ligand of 1 and 100 nM. (A) Binding plot was obtained by titrating ligand into a dilute solution of the IgG mixture. (B) Plot obtained when a dilute solution of ligand is held constant and the IgG mixture is added. The dotted lines in both (A) and (B) are the expected binding plots for the single IgG species.

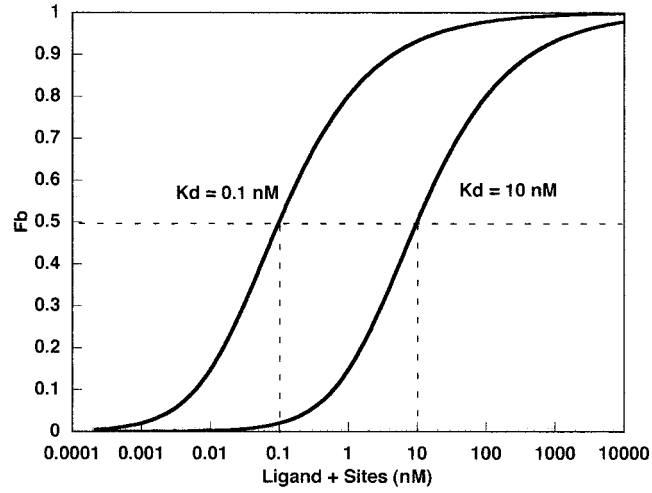

FIG. 4. Characterization of dilution dissociation curves for an equimolar mix of ligand and sites. The fraction of sites bound is plotted as a function of the sum of the ligand and site concentrations. Curves for dissociation constants of 0.1 and 10 nM are shown. A line is indicated for the 0.5 fraction dissociated point, and a drop line at each intersection point is drawn.

experimental data, it is often not possible to accurately calculate the fraction bound nor to reach complete saturation. These effects result in the saturation line being drawn below its true position.

The number of binding sites per IgG molecule is known and renders the stoichiometric binding experiment somewhat superfluous. However, if one already has knowledge of the stoichiometry, the same stoichiometric conditions can serve as an assay for the concentration of IgG in a given solution. The experimental protocol is identical to the example above, but the abscissa would read the amount of sample added per mole of ligand. The intersection point would then report the amount of sample containing the same moles of sites as moles of ligand in our solution from which the solution concentration of IgG would be simply determined.

In the above examples the ligand concentration was kept well above the dissociation constant. If the ligand concentration is too low, then at low protein concentrations there will not be complete binding and the stoichiometry line will have a reduced slope. The intersection of the lines, in this case, will overestimate the number of sites per protein molecule (Fig. 6). Repeating stoichiometry experiments at higher ligand concentrations should lead to identical estimates, if ligand concentrations are appropriate, and is a valuable check on the experimental results.

Error in K_d Determinations

The precision and accuracy of a ligand binding experiment are always research concerns. The accurate identification of error sources within an experimental protocol is an invaluable process that can help guide the researcher in the experimental design and in the eventual interpretation of the results. Unfortunately, the type and the extent of these errors are intimately tied to the experimental protocol, making the discussion of error technique-dependent. We can, however, identify some limits for certain errors common to ligand binding experiments.

Errors can be split into two types: systematic and random. Random error can be understood through statistics, such as the standard deviation of a mean value, and generally influences the precision of the resolved parameters. In contrast, systematic error biases results and leads to errors in accuracy. Systematic errors are particularly sinister because they appear as trends and can mimic "reasonable" results. Let us first examine a few points about random error elements in binding studies.

Random error. How does an error in the determination of the fraction bound, F_b, translate into an error in the dissociation constant? The relationship given in Eq. [9] can be used to calculate the propagation of error from F_b to the dissociation constant K_d. If we assume that the error in the determined ligand concentration is insignificant, then using basic error propagation rules for equations of a single variable (17), the general relationship between the error in F_b and error in K_d

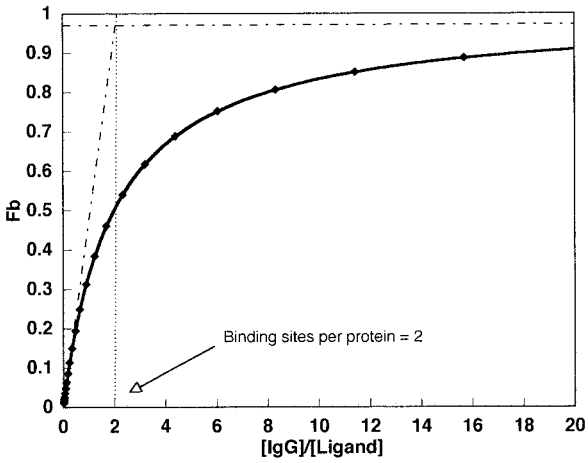

FIG. 5. A simulated stoichiometric binding plot for an IgG–hapten binding with a K_d of 1 nM. The hapten concentration was kept constant at 10 nM and the IgG concentration was varied. Dashed lines are drawn from slopes at the low and high protein concentrations. A reduced scale for the [IgG]/[Ligand] is used to emphasize the intersection point of the two lines and the estimation of the sites per IgG, 2. Ideally, the saturation line should be horizontal at $F_b = 1.0$. Here, to reflect many real experiments, saturation is not completely reached (0.97), and the resulting line is below the ideal position.

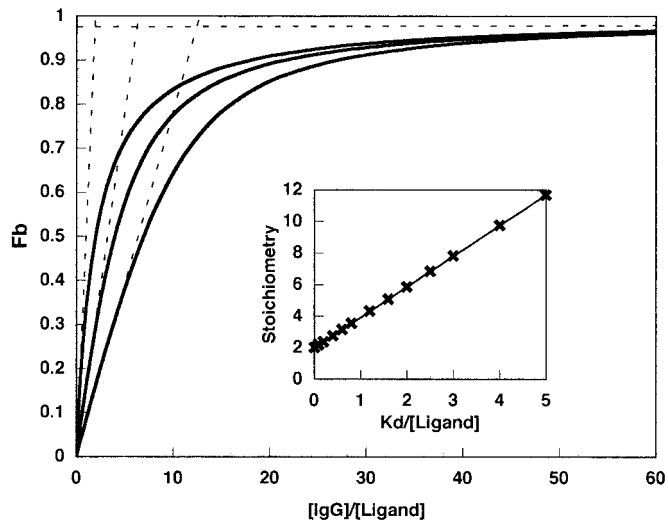

FIG. 6. Simulated curves demonstrating the influence of equilibrium conditions on an IgG stoichiometric binding experiment. Ligand was held constant and antibody was added to given an F_b range from 0.03 to 0.97. Data are plotted as F_b versus [IgG]/[Ligand]. The dissociation constant was 1 nM. Curves are drawn, left to right, for decreasing ligand concentrations of 10, 5, and 1 nM. Dashed lines are drawn for the saturating line and the stoichiometric line determined from the first and last two points, respectively. The intersection of the two lines is used to calculate the number of binding sites per protein from the abscissa. Inset: Plot of the stoichiometry determined as a function of the K_d ligand.

will be

$$\delta K_d = \left| \frac{dK_d}{d(F_b)} \right| \delta(F_b), \quad [13]$$

where dK_d and $d(F_b)$ are the standard deviations in the dissociation constant and fraction bound, respectively, and $dK_d/d(F_b)$ is the derivative of K_d with respect to F_b. The derivative is easily solved from Eq. [9] and the specific error relationship of interest is shown in the equation (drawn in Fig. 7)

$$\delta K_d = \left| \frac{-X}{F_b^2} \right| \delta(F_b). \quad [14]$$

The same relationship was derived by quadratic sum in an earlier work of Weber (18).

Graphed in Fig. 7A, Eq. [14] identifies two points about ligand binding data: the precision in our estimates of K_d is not constant across F_b, and the highest precision is held in the region around $F_b = 0.5$. The error in the estimated K_d increases from four times the error in F_b, at the minimum, to approximately six times at the $0.2F_b$ and $0.8F_b$ points. Though these estimates are for calculations with a single data point, one can use this information to assess how a particular error in data translates into precision in K_d. It is interesting to note that random error in F_b will lead to systematic error in K_d (Fig. 7B). This is due to the fact that binding curves are not symmetric, and an error in F_b will tend to push the apparent (fit) K_d to higher values (20).

In addition to understanding the single point error propagation, the number of collected data points is a critical factor in determining precision of a resolved dissociation constant. One can correctly intuit that the error in K_d can be reduced if more data are collected. How should one decide the number of data points necessary to achieve satisfactory results? In reality there is no single best number of points; the error in K_d decreases as more points are collected, so the number of points will depend on the required confidence for K_d. Information theory indicates that the maximum information occurs when points are spaced by $2d$ across F_b, where d is the standard deviation in the calculation of F_b (18). However, information content is more a measure of the resolvability in the data for model-dependent variables than an error in the determined parameters. From basic principles of error analysis we know that the statistical error in the determined binding constant is reduced by the square root of the number of points collected. This tenet can be easily demonstrated through simulating a large number of ligand binding data sets, adding a random Gaussian error to F_b, and then calculating the standard deviation of the resolved dissociation constants. Figure 8 shows the simulation results as a function of the number of data points collected per data set, spanning from 0.2 to 0.8 in F_b, for a binding interaction with a K_d of 1 nM and an error in F_b of ± 0.02. As one might expect, the more data points (p) per data set, the lower the standard deviation of K_d and the better the certainty. If we eliminate the error reduction due to the number of data points by multiplying the dK_d by $p^{1/2}$ (Fig. 8), then the intrinsic error in the measurement, as given by Eq. [14], should remain. We can estimate our expected error in K_d in the simulated data

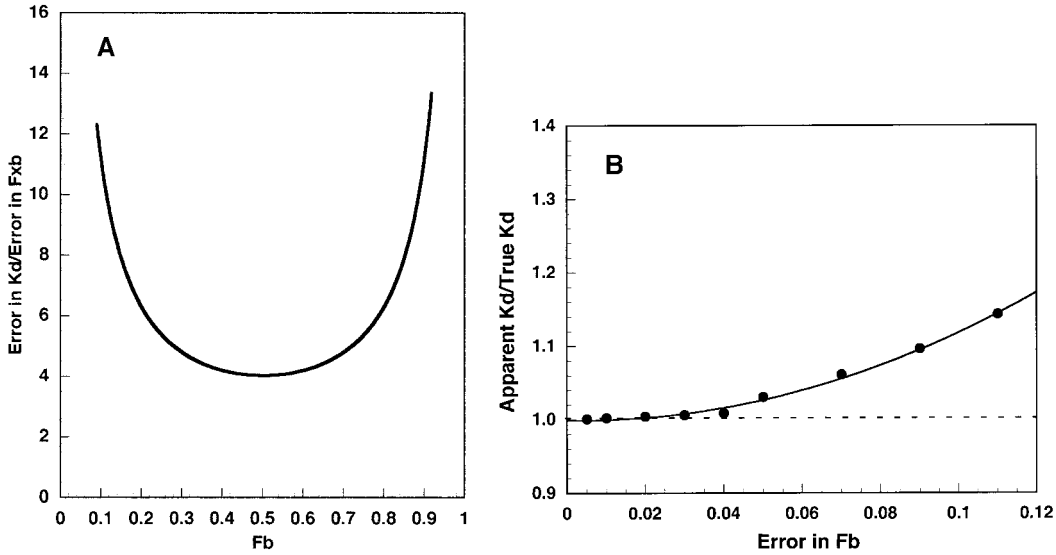

FIG. 7. (A) The error in K_d as a function of error in F_b. (B) The systematic deviation in K_d (apparent K_d/true K_d) as a function of error in F_b. Data sets ($n = 5000$) were simulated with a Gaussian error introduced into F_b. The sets for each error were then fit and the mean resolved K_d/true K_d was plotted as a function of the introduced error. A more rigorous simulation can be found in the literature (20).

from Fig. 7A at approximately 5 times the error in F_b. Our predicted standard deviation in K_d would then be 5×0.02 nM, or 0.1 nM. Indeed, our limit shown in Fig. 8 turns out to be 0.107 nM, very close to the predicted value. The small increase in certainty early in the plot is explained by the fact that finite numbers of data points do not properly sample the errors across the chosen region of F_b.

Systematic error. The source of error in ligand binding experiments is not restricted to random error. In any measurement there is always a contribution to the uncertainty, error that cannot be described by statistics. Systematic error is related more to the accuracy of the measurements and less to the precision of the measurements. The source of systematic error is highly dependent on the protocols used in preparing samples, the bias of the instruments, and the subsequent manipulations of the raw data to deliver the estimate of the fraction bound. The potential sources for systematic error vary greatly. In practice, the rule for dealing with systematic error is a pragmatic one: identify the error source and reduce its influence on the accuracy of the final result.

One obvious example of systematic error is in the accuracy of the measuring instruments used in preparing the samples. When aliquots of hapten are being added to an IgG solution, the consistent addition of too much or too little ligand will clearly shift the binding profile to the left or right. No amount of sampling can correct for this error. A less obvious, sample-dependent error is introduced by the presence of hapten in the preparation of IgG antibodies. Hapten-specific IgG antibodies are often purified by means of affinity chromatography, where the hapten is linked to a solid support and used to bind and elute the sought IgG. Unfortunately, elution of the antibodies from the support often requires harsh conditions, which can detach hapten and contaminate the IgG preparation. In a standard binding experiment, where ligand is progressively added to a solution containing a fixed IgG concentration, there will be an error in the concentration of ligand present as dictated by the amount of contaminating ligand. This error will affect the determination of the binding constant. If, on the other hand, IgG is titrated into a constant ligand concentration, the effects on the resulting binding plot are more subtle. As the IgG concentrations are increased, the concentration of free ligand will be progressively underestimated and the binding profile will be distorted.

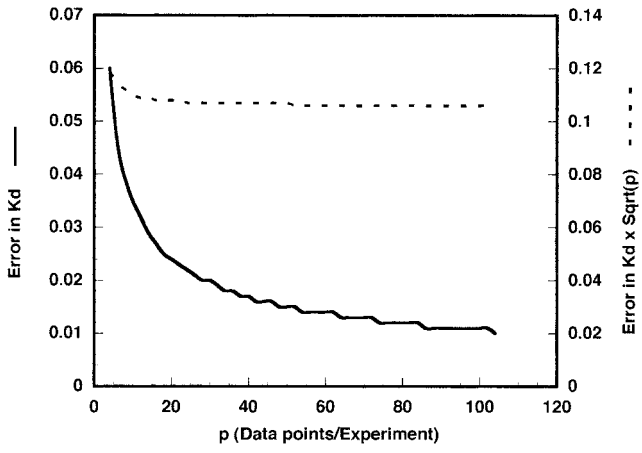

FIG. 8. The standard deviation in K_d is reported as a function of number of data points (p) per experimental set, spaced evenly from $F_b = 0.20$ to $F_b = 0.8$ (solid line). For each set, 2000 experiments were simulated with a Gaussian error (± 0.02) introduced into F_b. The standard deviations for the resolved K_d values were calculated and plotted. The curve of $K_d \times p^{1/2}$ versus p is given (dashed line) to illustrate the inherent error of a given data span without the signal-to-noise reduction due to the measurement of multiple points.

Other Graphical Analyses

In addition to directly fitting data to Eq. [10], several linear transforms of this equation are commonly used to evaluate binding data. The two most commonly used transforms are the double-reciprocal plot and the Scatchard plot (4). These transforms are

Double-reciprocal plot:

$$\frac{1}{F_b} = \frac{K_d}{nL} + \frac{1}{n} \qquad [15]$$

Scatchard plot:

$$\frac{F_b}{L} = \frac{n}{K_d} - \frac{F_b}{K_d}, \qquad [16]$$

where L is the free ligand concentration, n is the number of sites (again we are using the concentration of sites rather than protein and thus $n = 1$), K_d is the dissociation constant, and F_b is the fraction of sites bound. The purpose of these transformations is to linearize binding data and simplify the extraction of the binding parameters. In Fig. 9, data on the association of anti-theophylline IgG with fluorescein-labeled theophylline are shown. In this example, fluorescein-labeled theophylline (19) is held constant and the anti-theophylline IgG is added. The fraction bound is then determined and the data are plotted in standard form (A), in double-reciprocal form (B), and in Scatchard form (C). Analyses of the dissociation constant, K_d, and the stoichiometry, n, are given in each of the figures. To illustrate the potential for errors in using these linear transformations, we chose to plot data in Fig. 9 that have a sensible amount of error and that cover a broad range of the binding profile. In some cases, researchers will eliminate what they consider statisti-

cally meaningless points and the accuracy of their results may be improved, but the subjective elimination of points has obvious dangers. In the data presented above, the low F_b points contain most of the apparent error and might be removed. The accuracy of the fits to the adjusted data set is improved, but the analysis still shows significant error in the resolved K_d and n. Elimination of data points has the unfortunate function of also eliminating information. If one must use the linear equations, then the data should be weighted to correct for the errors induced through transformation (20).

The use of the linear transformations is not recommended. Today, with easy access to computers and the availability of many curve-fitting software applications, there is no need to linearize Eq. [9]. It is important to keep in mind that transformed data contain no new information; stoichiometries and binding constants can be resolved through fitting with Eq. [8], [9], or [10].

EXPERIMENTAL METHODS

Absorption Spectroscopy

Absorption spectroscopy can provide important information about the type and character of interactions between a ligand and the corresponding antibody binding site. Absorption spectra of a hapten and/or antibody often demonstrate pronounced changes on binding. For example, anti-fluorescein antibodies may shift the absorption maximum of fluorescein as much as 35 nm to longer wavelengths in the antibody–hapten complexes. Such shifts reflect changes in the fluorescein environment and its interactions with contact residues in the antibody binding site (21, 22). For several antibody systems, such as anti-opiate monoclonal antibodies (mAbs) (23) and anti-guanidinium sweetener mAbs (24), the appearance of a charge transfer band at 350 nm is characteristic of the bound antibody. With absorption data it is often possible to pinpoint a specific amino acid side chain in the antibody binding site directly involved in the hapten interaction (25).

Unfortunately, application of absorption spectroscopy to the evaluation of antibody–hapten equilibrium binding constants is limited. This restriction comes from the relatively low sensitivity of the method. Even with the best quality instruments, it is an experimental challenge to record a spectrum with peak absorbance below 0.01 OD unit with adequate precision. Usually, molar extinction coefficients for small haptens are in the range of 10^3 M^{-1} cm^{-1}. For some highly

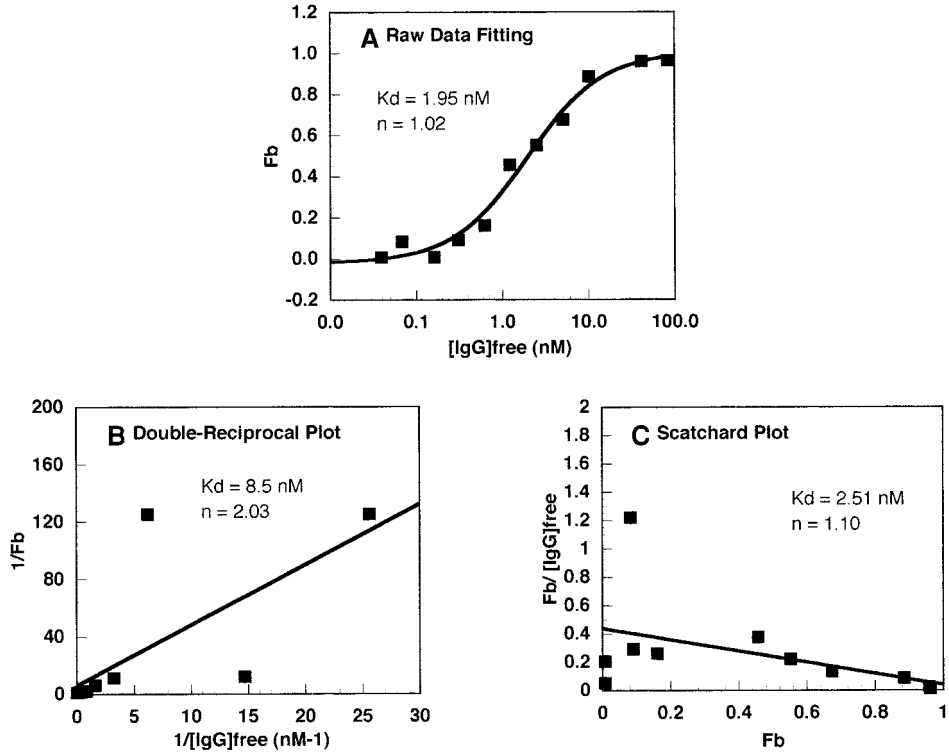

FIG. 9. Theophylline and anti-theophylline IgG binding data graphed as (A) raw data fitted to Eq. [10], (B) double-reciprocal plot fitted with Eq. [15], and (C) Scatchard plot fitted to Eq. [16]. The data set was chosen to exaggerate the defects in fitting with the linear transformed equations. The actual stoichiometry, n, is 1 and the dissociation constant should be 2 nM. The fit to Eq. [10] (A) is the superior fit. For the transformed equations, the estimates of K_d were particularly inaccurate. If the low F_b points are eliminated, the accuracy is improved but remains poor. Proper weighting, of course, can compensate for the data transforms in (A) and (B) and deliver accurate K_d estimates.

aromatic haptens such as fluorescein and rhodamine derivatives, it can range as high as 1.1×10^5 M^{-1} cm^{-1} (26). However, even the highest possible extinction coefficients combined with the most sensitive instrumentation do not allow dilution of such haptens to concentrations below 0.1 μM. Given these restrictions, the operational range for K_d determination by methods of absorption spectroscopy has a limit of 10^{-7} M. In practice, such sensitivity can be achieved only for antibody–hapten systems with strong absorption of the hapten at visible wavelength regions and well-separated spectra of the free and bound forms. An example is illustrated in Fig. 10, where hydroxyphenylfluoron, a fluorescein derivative, is titrated with an anti-fluorescein antibody.

When absorption spectra of the bound and free hapten overlap, antibody binding experiments become more difficult. Certain modifications can enhance the sensitivity of absorption techniques and help to overcome the aforementioned restrictions. Application of differential spectroscopy to the situation with overlapping spectra may provide marginal improvement in resolution for conducting binding experiments. Increasing the optical path lengths to 10 cm or to even longer capillary cuvettes can increase the sensitivity of absorption methods by an order of magnitude or so. On a practical note, careful correction for light scattering (27) is mandatory for all absorption measurements. Such correction may eliminate long-wavelength shoulders in absorption spectra that could be misinterpreted as indications of the binding-induced charge transfer effect. Programs using multiwavelength spectroscopic data analysis and a global fit approach can also be very helpful in processing binding data and eliminating spectral artifacts (SPECFIT, Spectrum Software Associates, Chapel Hill, NC; SpectraBind (28)).

Circular Dichroism

Circular dichroism (CD) is a spectroscopic technique based on the difference in absorption of left and right circularly polarized light. Therefore, in binding experiments CD possesses all of the advantages and limitations of absorption spectroscopy. CD can provide important structural information, but like other absorption techniques it has relatively low sensitivity. As a rule, hapten binding does not affect antibody secondary structure, and CD spectra of antibodies in the far-UV region (170–240 nm), where the peptide bond is the dominating chromophore, do not show changes on binding. It is possible to expect the appearance of new CD bands in the area of hapten absorption and in the near-UV region, 250 to 320 nm, where protein absorption is caused by tryptophan, tyrosine, and phenylalanine side chains. These residues are found in close proximity to the hapten in the majority of antibodies. CD bands that appear on binding to the hapten are known as induced, or extrinsic, CD effects.

A strong extrinsic CD signal (Fig. 11) in the region of 400–600 nm is observed for several anti-fluorescein antibodies (29, 30). Fluorescein is not an optically active compound, but it demonstrates induced optical activity when bound to the antibody binding site. This type of induced CD spectrum has the same shape as the absorption band of coupled chromophores and, according to Strickland (31), such spectra may arise from nongenerative exciton coupling. The intensity of an extrinsic CD band is proportional to the product of the dipole strengths of coupled electronic transitions. The highest amplitude of the induced CD signal can be obtained when two aromatic rings are parallel, but the vectors of coupling transitions are displaced by a 45° angle (32). The distance for such interactions is as-

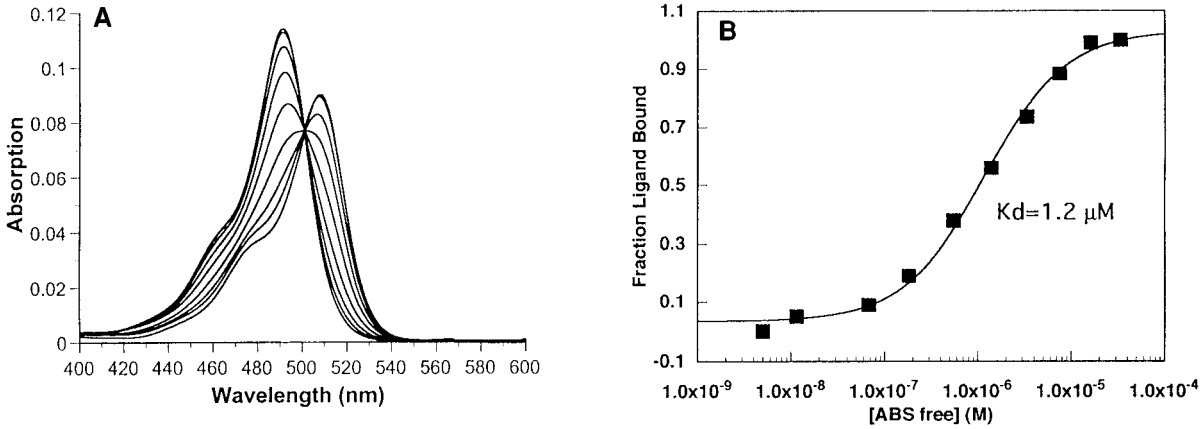

FIG. 10. Binding of 6-hydroxy-9-phenylfluoron (HPF) with mAb 9-40. Absorption spectra (A) were recorded on a Cary 4 Bio spectrophotometer (Varian Optical Spectroscopy Instruments, Mulgrave, Victoria, Australia) in a 1-cm cuvette. Concentration of HPF was 1.4×10^{-6} M. All spectra were individually corrected for light scattering. Absorption at 525 nm was used to calculate fraction hapten bound. Data (B) were fitted with Eq. [10]. An identical binding constant was also obtained from multiwavelength data analysis using SPECFIT software. Purified IgG 9-40 was kindly provided by Dr. James N. Herron (University of Utah).

sumed to be in the range of 10 Å or less (31). The appearance of CD bands in the near-UV region for the ligand-complexed mAb also indicates a specific geometric arrangement of the hapten and the binding site aromatic residues. Calculation of the CD difference spectra (bound minus free) of stoichiometrically bound antibody–ligand complexes allows visualization of the net spectral changes. In our study of antibodies that bind trisubstituted guanidinium sweetener (33), we suggested that the *p*-cyanophenyl moiety of the ligand acts as a molecular pointer in the CD spectra and identifies contact aromatic residues L:96W or L:96Y in the antibody binding pocket (Fig. 12).

Extrinsic CD bands are inherent only for an antibody–hapten complex. Such spectral data could be a perfect monitor of binding for the evaluation of binding constants. However, as we already mentioned, CD has restricted sensitivity. Its application depends on the antibody–hapten system, and, in general, the method can be recommended for determination of dissociation constants that are no lower than 10^{-7} M.

Fluorescence Spectroscopy

Fluorescence spectroscopy has proven to be a powerful tool in the study of molecular interactions and macromolecular dynamics. Fluorescence of a fluorophore can be influenced by many environmental factors such as viscosity, solvent polarity, temperature, local quenching groups, and local pH. In ligand binding studies, the nature of the changes in the signal is often less important than the correlation of the changes with the binding events. However, understanding the origin of these fluorescence changes can provide us with valuable information on the binding mechanisms and help to clarify the ligand-associated structural perturbations of the antibody, or biomolecule, binding site.

The primary advantages offered by fluorescence spectroscopy to ligand binding studies are its high sensitivity and the fact that samples can be examined in physiological buffers at equilibrium. Two fluorescence approaches that have been particularly useful in antibody–hapten binding studies are fluorescence quenching and fluorescence polarization. Below, we discuss the application of these techniques to specific antibody–ligand systems. We have also included a short discussion on the use of fluorescence correlation spectroscopy (FCS), which in the past few years has seen renewed interest.

Fluorescence Quenching

Interaction of an antibody with the hapten may change the intensity of the antibody's intrinsic fluorescence. Conversely, binding to the antibody may change the fluorescence intensity of a fluorescent hapten or hapten with an incorporated fluorophore. Thus, binding assays for antibody–hapten systems have been based on either hapten quenching or antibody quenching phenomena.

Fluorescence quenching (Q) is calculated by the formula

$$Q(\%) = \left(1 - \frac{I_{\text{sample}}}{I_{\text{free}}}\right) \times 100, \qquad [17]$$

where I_{free} and I_{sample} are fluorescence intensities of the component (antibody or hapten) before mixing and the sample with both components present, respectively. Some fluorophores show an increase in fluorescence when bound at the antibody binding site. A sign change in Eq. [17] will adapt it for fluorescence enhancement. Under the assumption that the observed change in fluorescent intensity is proportional to the fraction of bound component, Eq. [10] can be used to fit the data. The scaling factor m in Eq. [10] will be equal to the

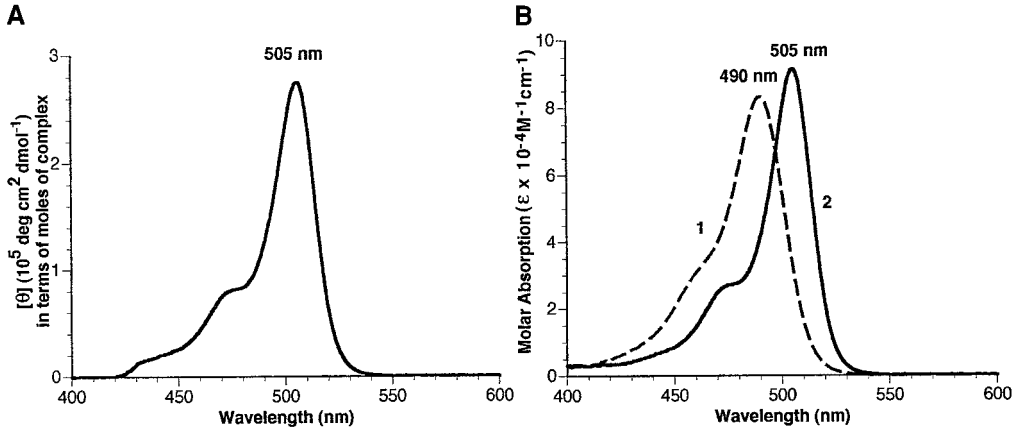

FIG. 11. Extrinsic CD effect (A) induced by mAb 4-4-20. Fluorescein (13 μM) is stoichiometrically bound by equimolar (in terms of binding sites) concentrations of IgG. For comparison, absorption spectra (B) of the free (1) and bound (2) hapten are also shown. Reprinted with permission from *Biochemistry,* 1992, **31,** pp. 12029–12034. Copyright 1992 American Chemical Society.

quenching (or enhancement) value at saturation (Q_{max}) and the constant factor c should to be close to zero.

As a rule, the observed change in fluorescence intensity of antibody–hapten complexes is accompanied by increase in fluorescence polarization. We discuss this effect in the next section. Here, it is important to recognize that the emission monochromator in the fluorometer has a wavelength-dependent, nonlinear efficiency for transmitting vertically and horizontally polarized light. Consequently, increased sample polarization on hapten binding will unevenly weight the fluorescence intensity measured in a binding titration. In the simple binding model discussed here, such experimental error will affect the slope of the linear correlation between the fluorescence change and the fraction of the bound component. Setting the polarizers to the appropriate "magic angle" conditions (see Appendix) corrects for this polarization effect. Another way to monitor changes in fluorescence intensity in the binding experiment is to calculate the G-factor-corrected total intensity value (see section on polarization and the Appendix) obtained from single wavelength polarization measurements.

A binding-induced spectral shift and a shape change in the fluorescence spectrum are more severe problems in data analysis. Often these distortions are minimal but, if present, can destroy the linear relationship between the observed fluorescence intensity and the fraction of bound component. To reduce this problem, it is possible to collect the fluorescence through an optical filter, rather than through a monochromator, and so measure the complete emission of both free and bound species. One may also scan the emission spectra under magic angle conditions and use the integrated emission as the total fluorescence intensity. In a more complicated situation, when the excitation spectrum is also affected, the data should be processed with programs designed for spectroscopic data and a global fitting approach used to properly extract the binding parameters (SPECFIT, Spectrum Software Associates; SpectraBind (28)).

Tryptophan is the primary intrinsic fluorophore in proteins and is often useful in binding studies. Tryptophan emission is highly sensitive to the microenvironment, which makes it an ideal intrinsic probe for monitoring changes in the local protein structure. The only other significant protein fluorophore is tyrosine, occasionally used for binding studies but generally less suitable for fluorescence measurements because of its low extinction coefficient, poor quantum yield, and low

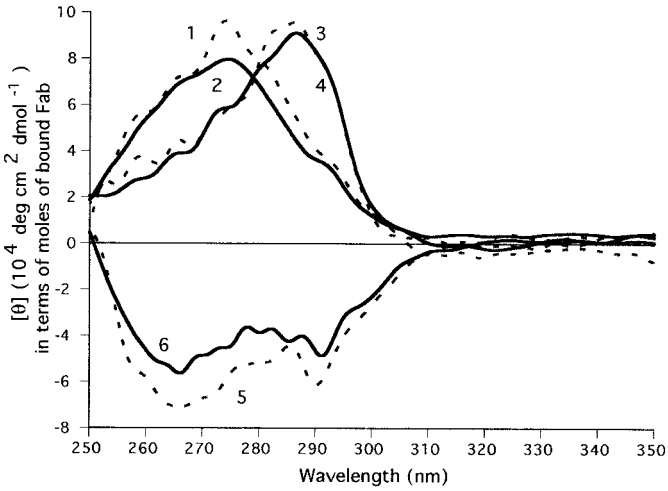

FIG. 12. Difference spectra (ligand complexed minus uncomplexed) and near-UV CD spectra of Fab fragments (solid lines) and IgG (dashed lines) from mAb: NC6.8 (spectra 1, 2); NC10.8 (3, 4); NC10.14 (5, 6). Antibodies NC 6.8, NC10.8, and NC10.14 bind the sweetener ligand *N*-(*p*-cyanophenyl)-*N′*-(diphenylmethyl)guanidine acetic acid with dissociation constants of 5.3×10^{-8}, 5×10^{-9}, and 7.3×10^{-8} M, respectively. Antibody binding site concentrations were maintained in the range of $5–10 \times 10^{-6}$ M and the concentration of the ligand in the range of $1–2 \times 10^{-5}$ M in all experiments. More than 99% of the binding sites were occupied (stoichiometrically bound) under these experimental conditions (see Eq. [6]). Because the free ligand does not possess any intrinsic optical activity, all changes in CD spectra on binding were induced by formation of the Fab–ligand complex. Expression of these CD spectral results in terms of the concentration of the bound Fab (which is essentially equal to the total Fab concentration in our experiments) allowed us to compare CD spectra of uncomplexed and ligand-complexed Fab fragments. Reprinted with permission from *Biochemistry*, December 1996, **35,** pp. 12029–12034. Copyright 1996 American Chemical Society.

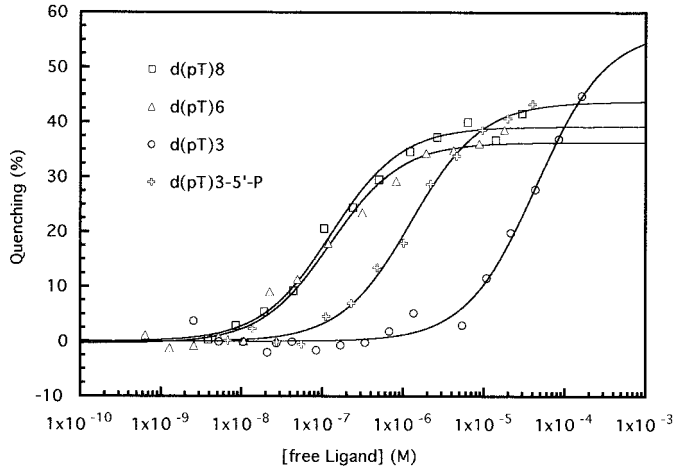

FIG. 13. Binding plots of oligodeoxythymidines and IgG 04-01. Quenching of protein fluorescence is shown as a function of free oligonucleotide concentration. Total concentrations of antigen binding sites (ABS) for $d(pT)_3$-5′-OH, $d(pT)_3$-5′-phosphate, $d(pT)_6$, and $d(pT)_8$ were 5.3×10^{-7}, 5.7×10^{-7}, 3.9×10^{-7}, and 2.9×10^{-7} M, respectively. Emission spectra were obtained using an ISS Greg PC (ISS, Champaign, IL) photon-counting spectrofluorometer equipped with prism polarizers. Emission spectra of protein intrinsic fluorescence were taken in region of 315–460 nm on excitation at 295 nm. Excitation and emission bandpasses were 8 and 16 nm, respectively. Reprinted with permission from *Biochemistry*, December 1993, **32,** pp. 9011–9017. Copyright 1993 American Chemical Society.

sensitivity to environmental factors. Early application of tryptophan and tyrosine fluorescence in biochemical studies can be attributed to Weber (34, 35), whose research promoted the use of intrinsic fluorophores in protein biophysics (see recent review by Callis (36)).

Location of tryptophan residues in or near a protein binding site creates conditions causing ligand-induced changes in intrinsic protein fluorescence. Aromatic amino acid residues are preferentially located on the intervariable domain surfaces of antibodies, including the area of the antigen binding site (1). In antibodies directed against planar haptens, such as fluorescein and trisubstituted sweetener ligands, tryptophan and tyrosine residues build up the actual "walls" of the binding pocket (22, 37, 38). In these antibodies, interaction of the hapten with the binding site substantially changes tryptophan fluorescence. This effect can be used to determine the extent of free and bound hapten and thus the stoichiometry of binding and the equilibrium binding constant.

Velick *et al.* (39) were the first to report the use of hapten-dependent quenching of antibody fluorescence for determination of the binding constant of rabbit anti-DNP antibodies toward 2,4-dinitrophenyl (DNP). Their work led to the discovery of the important immunological phenomenon "affinity maturation" (40), which was explained later by antigen-driven somatic hypermutations in variable regions of antibodies (41, 42).

We applied a similar experimental approach to the study of autoantibody BV 04-01, which binds single-stranded (ss) DNA (11), and to the work with antibodies against trisubstituted sweetener ligands (43).

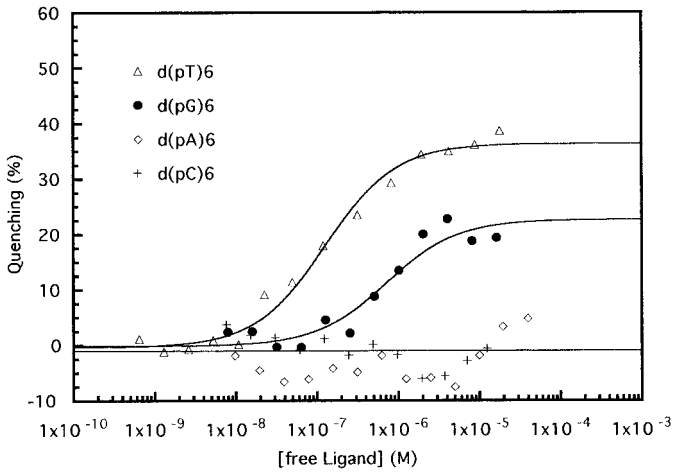

FIG. 14. Binding plots of different oligohomonucleotides and IgG 04-01. Quenching of protein fluorescence is shown as a function of free oligonucleotide concentration. Total concentrations of antigen binding sites (ABS) for $d(pT)_6$, $d(pG)_6$, $d(pA)_6$, and $d(pC)_6$ were 3.9×10^{-7}, 4.3×10^{-7}, 5.6×10^{-7}, and 4.9×10^{-7} M, respectively. Reprinted with permission from *Biochemistry*, December 1993, **32,** pp. 9011–9017. Copyright 1993 American Chemical Society.

Adapted from the former study, Figs. 13 and 14 and Table 1 illustrate binding of various unlabeled synthetic oligohomonucleotides by mAb BV 04-01. Data were obtained from measurements of tryptophan fluorescence of the antibody on titration with oligonucleotides, and the best-fit curves were drawn as the result of fitting with the simple binding model (Eq. [10]).

As shown in Fig. 14 reliable binding data can be obtained when only a fraction of the fluorescence is quenched. For example, hexadeoxyguanidylate quenched only 23% of antibody fluorescence at the saturation point.

Antibody BV 04-01 binds trideoxythymidylates with low affinity; therefore, a high ligand concentration is required to approach the saturation level. At these concentrations trideoxythymidylates begin to absorb the excitation light, resulting in an apparent loss of fluorescence, unconnected to binding. Such a phenomenon, known as the inner filter effect, can be minimized through the use of short path-length cells, or data need to be mathematically corrected (see Appendix). Nevertheless, it was technically difficult to reach a saturation limit with trideoxythymidylates, and therefore, we could not be confident of the quenching value for the completely bound antibody. To overcome this problem, we fitted the data through an iterative procedure described earlier. From the analysis, the saturation quenching value, the free ligand concentrations along the titration curve, and the dissociation constant were determined.

Additionally, we were able to refine the binding parameters of mAb BV 04-01 and different oligonucleotides (see Table 1). We confirmed a previous report that the hexamer is the minimum length oligodeoxythymidylate required for effective binding (44). We also found that BV 04-01 binds hexadeoxyguanidylate

TABLE 1

Quenching of Intrinsic Protein Fluorescence and Dissociation Constants of BV 0401 and Oligodeoxynucleotide Ligands[a]

Antibody and ligand	Q_{max} (%)	K_d (μM)	ΔG (kcal/mol) (association)
IgG 0401			
dT_3-5′-OH	56.9 ± 3.7	44.2 ± 7.6	−5.8 ± 0.1
dT_3-5′-phosphate	43.8 ± 1.0	1.25 ± 0.13	−7.9 ± 0.1
dT_6-5′-OH	36.7 ± 0.2	0.13 ± 0.02	−9.3 ± 0.1
dT_8-5′-OH	39.2 ± 1.4	0.13 ± 0.02	−9.3 ± 0.1
dG_6-5′-OH	22.7 ± 2.2	0.71 ± 0.31	−8.2 ± 0.3
dA_6-5′-OH	—	>100	—
dC_6-5′-OH	—	>100	—
SCA 0401/212			
dT_6-5′-OH	76.3 ± 6.5	3.21 ± 0.89	−7.4 ± 0.2
dT_8-5′-OH	70.9 ± 1.9	1.60 ± 0.17	−7.8 ± 0.1

[a] Reprinted with permission from *Biochemistry,* December 1993, **32,** pp. 9011–9017. Copyright 1993 American Chemical Society.

[$(dG)_6$] with an affinity comparable to that of oligodeoxythymidylates, a result not observed in binding experiments using radioimmunoassays. Comparison of the binding information with the three-dimensional structure of BV 04-01 (45) and the results from site-directed mutagenesis studies (46) allowed us to refine the structure–function relationships between mAb BV 04-01 and its ligands. In fact, the quenching data confirmed the critical role of the antibody heavy-chain Trp-100a residue in interactions with oligonucleotides. Differences in fluorescence quenching value at saturation (Q_{max} in Table 1) indicated distinct arrangements of the various oligonucleotides with contact amino acid residues and demonstrated conformational adaptability of BV 04-01 binding site and ssDNA.

In the hapten-induced fluorescence quenching of antibodies against trisubstituted sweetener, we were able to determine dissociation constants in the nanomolar range, significantly lower than those in the above examples (43). Figure 15A shows typical quenching effects of mAb NC10.14 on interaction with the sweetener *N*-(*p*-cyanophenyl)-*N′*-(diphenylmethyl)guanidine acetic acid. The corresponding binding plot for this system is given in Fig. 15B.

The sensitivity of an experimental determination of a binding constant based on quenching of intrinsic antibody fluorescence depends on the number of tryptophan residues in or near the antibody binding site and the extent of their quenching on ligand binding. Because of an abundance of tryptophan residues in antibody variable domains, this approach can work reasonably well for various antibody systems. Usually, ligand-induced tryptophan quenching is substantially greater in binding-site-containing fragments (e.g., Fab or Fv). In these proteins, the contribution of nonbinding site tryptophan fluorescence is reduced to give a greater fraction of the quenched signal (see single-chain antibody SCA 04-01/212 in Table 1) and an improved signal-to-background difference. Combined with an optimized experimental setup (for example, replacement of the emission monochromator with an appropriate bandpass filter will increase instrument throughput), utilization of such fragments may permit determination of subnanomolar dissociation constants.

In addition to binding parameters, structural information can be obtained through an understanding of the mechanism of a ligand-induced quenching effect. DNP-induced quenching of tryptophan fluorescence in anti-DNP antibodies revealed the presence of tryptophan residues at the antibody binding site and has been explained by the energy transfer between excited tryptophan(s) and DNP ligand (39). For anti-DNA antibodies and antibodies to trisubstituted sweetener ligands, conditions for resonance energy transfer do not exist. Quenching in this case could occur by direct interaction of the tryptophan residue(s) with the ligand or, indirectly, on ligand-induced conformational adaptation of the binding site by pulling tryptophans closer to local quenching groups. Intradomain disulfide bonds are likely groups because they are the strongest intrinsic quenchers of protein fluorescence (47). Other events like hydrogen bonding, excited-state proton, or electron transfer between tryptophans and the hapten or between tryptophans and other amino acid residues in the protein interior could also account for the observed quenching effects (48–50). Analysis of additional fluorescence data, e.g., comparison of emission and excitation spectra of free and hapten-bound antibody, may help to define the specific changes in tryptophan environment induced by hapten. Thorough analysis of the interrelations between the fluorescence data and the antibody's three-dimensional structure helps to pin-

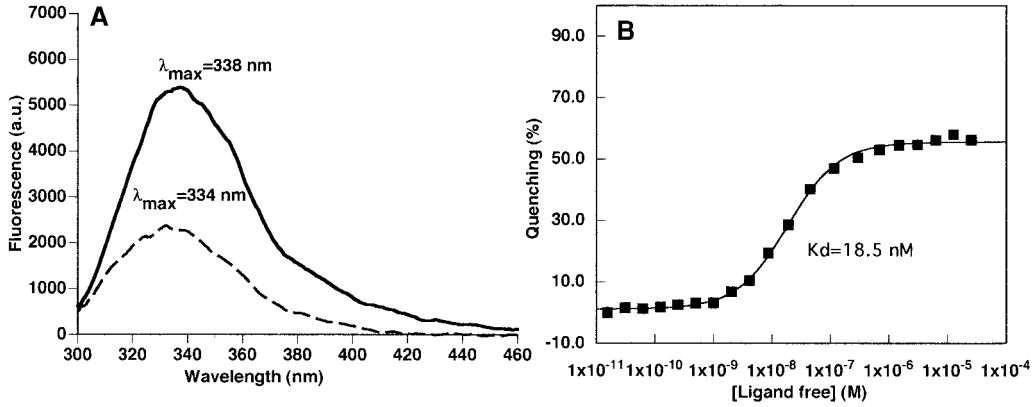

FIG. 15. (A) Intrinsic fluorescence of mAb 10.14 in free form (solid line) and saturated (dashed line) with ligand *N*-(*p*-cyanophenyl)-*N′*-(diphenylmethyl)guanidine acetic acid. Excitation was at 295 nm and band paths were set to 1 nm. The concentrations of the IgG and the ligand were 0.23 and 16 μM, respectively. Spectra were obtained using an SLM 8100 photon-counting spectrofluorometer with prizm polarizers set to the "magic angle." (B) Titration of mAb 10.14 with the ligand. The concentration of the antibody binding sites was 16 nM. Excitation was at 295 nm, emission was collected at 340 nm, and bandpasses were set to 8 nm. Reprinted with permission from *Biopolymers*, 1995, **39,** 395–406. Copyright 1995 John Wiley & Sons, Inc.

point the tryptophan residue(s) responsible for the observed spectral changes and suggests the conformational shifts that could effect such a change.

Additional information can be also obtained from fluorescence lifetime measurements. In fluorescence quenching studies, intensity changes reflect both dynamic and static mechanisms of quenching, which in turn identify specific characteristics of the hapten–antibody complex. These two mechanisms can be distinguished through a comparison of steady-state and fluorescence lifetime experiments. Whereas steady-state intensity quenching reflects both mechanisms, changes in fluorescence lifetime exclusively delineate a dynamic, diffusion-based quenching (see review by Eftink (51)). In the anti-ssDNA antibody BV-0401 system, the difference in fluorescence quenching efficiencies observed in fluorescence lifetime and steady-state measurements revealed that static quenching was the primary quenching component. Applying this information to the reported three-dimensional structure of mAb BV 04-01 (45), we were able to conclude that the intercalation of the ligand's thymine base between Tyr-32L and Trp-100aH planar rings may result in the formation of a dark complex and account for this static quenching component.

Quenching of fluorescent haptens is also used extensively in antibody binding studies. As a rule, fluorescent haptens developed for antibody structure–function studies or immunoassays are designed to exhibit high extinction coefficients and high quantum efficiencies. For this reason, they are extremely bright and can be used for the determination of the binding constants in the picomolar range. To exemplify application of fluorescent haptens in affinity measurements, we include experiments with two different antibody systems. The first example is the extensively studied anti-fluorescein mAb 4-4-20 (22, 37, 52). As shown in Fig. 16 this antibody quenches 96% of fluorescein fluorescence. In the second example shown in Fig. 17, the original hapten, digoxin, is labeled with fluorescein as a fluorescent reporter group (19). Binding of this conjugate by the anti-digoxin antibody involves interactions between the binding site and the fluorescein moiety and results in 53% fluorescence quenching. Both antibodies bind haptens with subnanomolar dissociation constants. The same considerations that we have made in studies using antibody fluorescence can be applied to experiments with fluorescent haptens. In addition to an understanding of the quenching mechanisms, studies with modified ligands contain important structural information. Fluorescence quenching data combined with measured binding constants may provide a researcher with complete characterization of the binding pair.

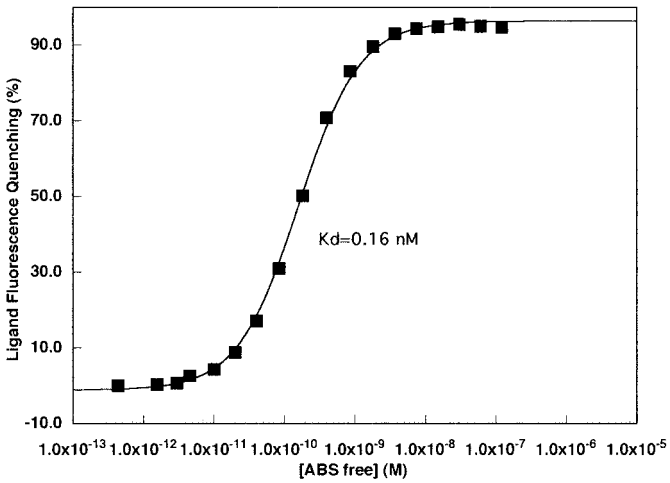

FIG. 16. Determination of the dissociation constant of anti-fluorescein mAb 4-4-20 and fluorescein (Molecular Probes, Inc., Eugene, OR) by measuring the hapten quenching. Concentration of fluorescein was 1.1×10^{-10} M. The experiment was conducted in 0.1 M phosphate buffer, pH 8.0. The quenching values were calculated from the total intensity data obtained in the single point polarization measurements on an SLM 8100 photon-counting spectrofluorometer. Excitation was at 470 nm with band path set to 4 nm. Emission light was collected through a 530-nm (25-nm bandwidth) optical filter (Schott Glass Technologies Inc., Duryea, PA). IgG 4-4-20 was purified on a protein A–Sepharose column (Pharmacia Biotech Inc., Piscataway, NJ). The hybridoma cell line 4-4-20 was kindly provided by Dr. D. M. Kranz (University of Illinois at Urbana-Champaign).

Fluorescence Polarization

Fluorescence polarization is sensitive to changes in fluorophore rotational motions and hence useful in monitoring antibody–hapten association. Binding of a small hapten to a relatively large antibody decreases

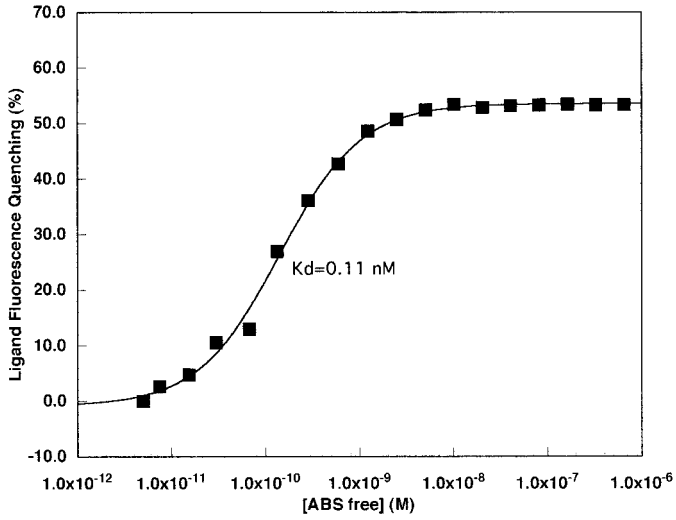

FIG. 17. Titration of the fluorescein-labeled digoxin (19) with anti-digoxin rabbit antibody. Concentration of the hapten was 8.1×10^{-11} M. The experimental conditions and instrument setup were identical to those given in the legend to Fig. 16. Antibody was purified from hyperimmune rabbit serum on a protein A–Sepharose column (Pharmacia Biotech Inc., Piscataway, NJ).

the rotational diffusion of the hapten molecule, thereby increasing the measured polarization of its fluorescence. Reciprocally, bound hapten may affect local motions of protein chromophores and change the polarization of intrinsic antibody fluorescence. The first situation is far more common than the latter and will be the focus of this section. Nevertheless, the following considerations are also appropriate for the situation when a hapten-induced increase in the polarization of antibody intrinsic fluorescence is used to monitor binding.

Haptens labeled with fluorescent reporter groups are used extensively in various areas of immunology, especially in antibody structure–function studies and immunoassays. Often, the binding of such ligands does not affect the emission intensity, and an increase in fluorescence polarization may be the only detectable spectroscopic feature available for monitoring binding.

In 1952 Gregorio Weber published general principles for application of the fluorescence polarization approach to studying macromolecules (53a,b). On the basis of the Perrin equation for fluorescence depolarization of a spherical particle (54), Weber formulated the addition law, which relates polarization of a mixture of fluorophores to the individual components present in solution,

$$\left(\frac{1}{\bar{P}} - \frac{1}{3}\right)^{-1} = \sum_i \frac{f_i}{(1/P_i - 1/3)}, \qquad [18]$$

where $\bar{P}$ is the polarization of the mixture, P_i is the polarization of each fluorophore, and f_i are the fractional fluorescence intensities of fluorophores. In these two papers, Weber also described the experimental determination of polarization of macromolecules in solution and introduced labeling of proteins by conjugation with fluorescent dyes. This work opened a successful era for implementation of fluorescence polarization in biochemistry.

Later, the same addition law was expressed in terms of anisotropy (55),

$$r = \sum_i f_i r_i, \qquad [19]$$

where r is the anisotropy of the mixture, r_i is the anisotropy of the ith fluorophore, and f_i are the fractional fluorescence intensities (their sum is equal to 1). Definitions of the terms polarization and anisotropy can be found in the Appendix. These similar concepts are interconvertible, and both terms are popular in the literature. At present, many researchers prefer to express binding data in terms of anisotropy because of its simplicity in mathematical manipulations (for a general review see Lakowicz (56)).

Anisotropy (r) at any point in the titration is the sum of the products between the individual anisotropies of the free (r_{free}) and the bound (r_{bound}) species and their respective fractional intensities (f_{free} and f_{bound}; note that $f_{free} + f_{bound} = 1$) as given by

$$r = f_{free} r_{free} + f_{bound} r_{bound}. \qquad [20]$$

If fluorescence intensity of the hapten is not changed on binding to the antibody, the respective fractional contributions of the free and bound hapten will be equivalent to their fractional concentrations. Consequently, to calculate the molar fraction of the bound hapten from anisotropy measurements, Eq. [20] can be rearranged to solve for F_{bound} (F_b):

$$F_b = \frac{r - r_{free}}{r_{bound} - r_{free}}. \qquad [21]$$

Figure 18 presents such an example. Fluorescein-labeled digitoxin was titrated with the anti-digitoxin antibody and binding data were fitted with Eq. [10].

If antibody binding affects hapten fluorescence, fractional intensities of the free and bound hapten will show unequal weighting and will no longer be equivalent to the respective molar fractions. Equation [21] must then be modified by including a factor, q, to adjust for this weighting,

$$F_b = \frac{r - r_{free}}{(r_{bound} - r)*q + r - r_{free}}, \qquad [22]$$

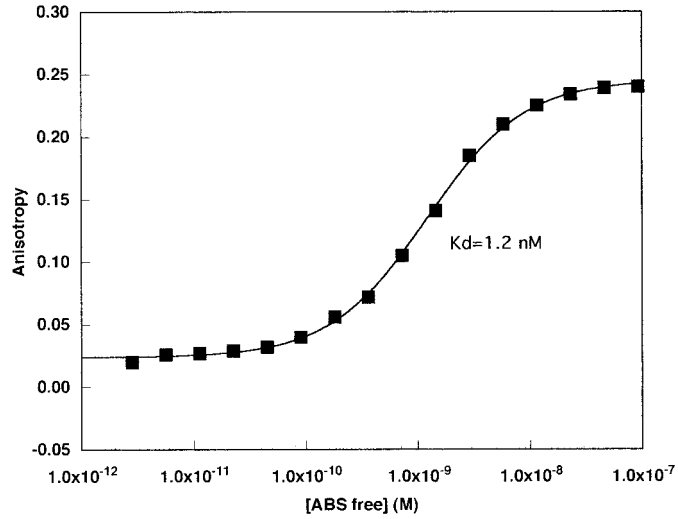

FIG. 18. Determination of the dissociation constant of anti-digitoxin rabbit antibody and digitoxin by anisotropy measurements. The concentration of the fluorescein-labeled digitoxin ligand was 0.22 nM. The experimental conditions and instrument setup were identical to those given in the legend to Fig. 16. Antibody was purified from hyperimmune rabbit serum on a protein A–Sepharose column (Pharmacia Biotech Inc., Piscataway, NJ).

where q is the ratio of fluorescence intensities of the bound and free hapten measured under the same experimental conditions. Because free and bound hapten possess different fluorescence intensities, anisotropy data cannot be directly fitted with Eq. [10]. It is necessary to first calculate the fraction of the bound ligand with Eq. [22] and then use Eq. [9] for fitting. Otherwise, it is possible to combine Eq. [22] with Eq. [9] to fit the anisotropy data directly.

The importance of the above correction is illustrated in Figs. 19 and 20, which show the binding plots obtained by anisotropy measurements in the earlier presented fluorescence quenching experiments (Figs. 17 and 16) with anti-digoxin and anti-fluorescein antibodies. Anti-digoxin antibody moderately (56%) quenches the hapten fluorescence, whereas anti-fluorescein mAb 4-4-20 quenches fluorescein hapten up to 96%. In the moderate example, anti-digoxin antibody, correction for quenching changes the determined K_d more than 2-fold. With anti-fluorescein antibody, similar correction results in a 13-fold difference. Notably, the most substantial correction occurs in the upper part of the binding curve, at high antibody concentrations, when the fraction of the bound hapten approaches saturation.

As mentioned at the beginning of this section, fluorescence polarization (or anisotropy) depends on the rotational diffusion of a fluorophore and is thus sensitive to the dynamics of macromolecules. The steady-state fluorescence anisotropy discussed here gives a weighted average of the rotational modes in the system studied. The more sophisticated measurement of time-resolved anisotropy can extract the individual rotational rates present in antibody–hapten complex. Because this technique is less likely to be used for evaluating binding constants, we will just note that time-resolved anisotropy measurements provide information about local motion of the bound hapten and rigidity of the antibody binding site. It is also possible to determine rotational rates of protein subunits and domains in such experiments. In fact, independent movements of the Fab fragments in the IgG molecule, the segmental flexibility of antibody in solution, were discovered by means of fluorescence polarization (57, 58).

Fluorescence Correlation Spectroscopy

Fluorescence correlation spectroscopy (FCS) is another method for studying dynamic processes of fluorescent molecules in solution. The method was introduced by Magde *et al.* more than 20 years ago (59–61), but had limited application in biological studies because of technical difficulties. Recent progress in the theory and practice of single molecule detection has revived the technique and made FCS equipment reliable. Rigler, Eigen, and co-workers (62–64) developed biological applications of FCS and commercially available instrumentation (Carl Zeiss Jena GmbH, Jena, Germany; EVOTECH BioSystems GmbH, Hamburg, Germany).

Basically, FCS measures fluorescence fluctuations in a small open volume of a solution, where fluorophore-containing molecules freely diffuse in and out. To register such fluctuations in solution with nanomolar concentrations of fluorescent molecules, the observation volume must be on the order of one femtoliter (10^{-15} L). Small observational volumes can be achieved using advanced confocal microscopes (64–67) or, alternatively, with two-photon excitation method (68). Spikes

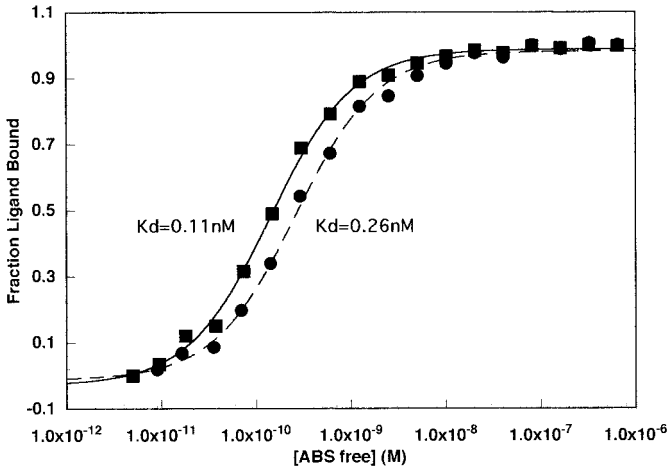

FIG. 19. Determination of the dissociation constant of anti-digoxin rabbit antibody and fluorescein-labeled digoxin by anisotropy measurements. Anisotropy data were obtained in the same experiment shown in Fig. 17, where the fluorescence quenching at saturation was 56%. The solid line represents the data properly corrected for the quenching of the ligand fluorescence.

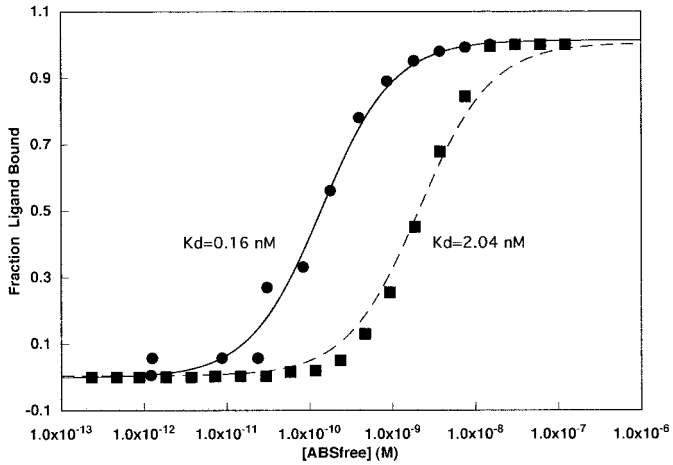

FIG. 20. Determination of the dissociation constant of mAb 4-4-20 and fluorescein hapten by anisotropy measurements. Anisotropy data were obtained in the same experiment presented in Fig. 16. Solid line shows the corrected results. This antibody quenches 96% of the hapten fluorescence.

of intensity over background, originating from single molecules, can be analyzed with the autocorrelation function. This number fluctuation analysis was originally introduced many years ago for measuring diffusion coefficients of colloidal particles in a fixed volume (68–70). The autocorrelation analysis gives information on both the rate at which particles diffuse in and out of the observation (or excitation in two-photon FCS) volume and the number of particles in this volume. The ability to measure the diffusion time, and therefore the translational diffusion coefficient, makes FCS perfectly appropriate for studying protein–ligand association. For antibodies and haptens, the equilibrium binding constants can be evaluated from diffusion parameters obtained in solution at equilibrium. To test the FCS technique, we studied the binding of several fluorescein-labeled haptens (theophylline, digoxin, digitoxin) with corresponding antibodies (71, 72). The experiments were carry out with the ConfoCor (Carl Zeiss Jena GmbH) instrument, which is based on a confocal fluorescence microscope, and a small air-cooled argon-ion laser (488-nm line) used for excitation. The intensity autocorrelation data were analyzed for multiple diffusional components with ACCESS software (EVOTECH BioSystems GmbH; Carl Zeiss Jena GmbH). Fractions of the free and bound hapten were determined for each point of the binding titration, and the dissociation constant was calculated. Comparison of the binding constants obtained in FCS experiments with those from the fluorescence polarization method showed excellent agreement. For example, the same samples of the titration of fluorescein-labeled digitoxin with anti-digitoxin antibody (Fig. 18) were examined by FCS. The FCS experiments gave a dissociation constant of 1.1 nM.

There are other approaches to evaluating FCS data. Palmer and Thompson (73) have used high-order fluctuation moments, and Gratton and co-workers (74) have developed the method of photon counting histogram (PCH). PCH was used to evaluate the binding constant of anti-digoxin antibody (75). The dissociation constant of 0.25 nM obtained by PCH analysis was in a good agreement with the result from fluorescence polarization experiment.

A new means for expanding the capabilities of FCS in studying macromolecular association and ligand binding is dual-color fluorescence cross-correlation spectroscopy, recently introduced by Rigler and co-workers (76) and Eigen and co-workers (77, 78). In this technique, two molecular species (i.e., protein and ligand) are labeled with different fluorescent dyes, and only the complex will produce the detected cross-correlated signal. Such an approach minimizes background interference and allows the detection of low concentrations of associated molecules. As a result, the cross-correlation approach improves the sensitivity of FCS by orders of magnitude.

With continued progress, FCS has a strong potential to become the method of choice in the determination of antibody–antigen binding affinities.

SUMMARY

We have attempted in this article to describe a variety of UV–VIS absorption and fluorescence techniques that can be used to study antibody–hapten associations. Clearly, these techniques are not limited to antibodies and can be used for other systems as well. In general, standard absorption methods, including circular dichroism, are not inherently sensitive enough for accurate determination of high-affinity binding constants. For systems with dissociation constants below 10^{-6} M, these methods are not suitable. Nevertheless, absorption techniques can be used in stoichiometry experiments in which antibody and hapten concentrations must be high. In contrast to absorption, fluorescence is an inherently sensitive methodology and has been a common choice for the determination of tight antibody–hapten binding constants. Among the various fluorescence protocols, techniques based on fluorescence intensity and fluorescence polarization measurements are the most common in ligand binding studies. In the future, we will likely be seeing more binding studies involving fluorescence correlation spectroscopy, considering the present interest in this technique.

APPENDIX

There are numerous sources of information on fluorescence spectroscopy containing detailed descriptions of the basic principles of fluorescence spectroscopy, experimental techniques, and equipment (for a general and broad discussion see Lakowicz (56)). Here, we provide the reader with definitions of terms we have used in the general text.

Polarization and anisotropy measurements. It is important to define our frame of reference in discussing polarization. By common agreement, the plane of the laboratory (or tabletop) is defined as the horizontal plane, and the vector normal to this plane is the vertical axis. When a standard sample polarization is being taken, the excitation light is polarized along the vertical axis. The emission is collected, as is routine in fluorescence spectroscopy, at right angles to the excitation path. The vertically and horizontally polarized emission intensities are measured separately and the

polarization (P) and anisotropy (r) are calculated using the equations

$$P = \frac{I_v - I_h}{I_v + I_h} \quad [23]$$

and

$$r = \frac{I_v - I_h}{I_v + 2I_h}, \quad [24]$$

where I_v is the emission intensity polarized along the vertical axis and I_h is the component of the emitted light polarized along the horizontal axis. It is also common in the literature to find two other subscript sets: $\parallel$ (parallel to the excitation light), or 0°, for the vertical axis and $\perp$ (perpendicular to the excitation light), or 90°, indicating the horizontal axis. Because the excitation light is generally set to vertical, this designation is often not indicated. However, one may see double symbols used to identify the polarization of the excitation and emission paths distinctly. Equations [23] and [24] can be rewritten as

$$P = \frac{I_{vv} - I_{vh}}{I_{vv} + I_{vh}} \quad [25]$$

and

$$r = \frac{I_{vv} - I_{vh}}{I_{vv} + 2 \times I_{vh}}, \quad [26]$$

where the subscript symbols, from left to right, designate the excitation and emission paths, respectively. As a rule, optical parts of fluorometers possess unequal transmission (monochromators, lenses, filters) or varying sensitivities (photodetector) for vertically or horizontally polarized light. Corrections for such instrumental artifacts are made through the use of a correction factor known as the G factor. The G factor is measured according to the equation

$$G = \frac{I_{hh}}{I_{hv}}, \quad [27]$$

with the excitation polarizer set at the horizontal position, a condition under which the horizontally and vertically polarized emission intensities should be equal.

Equation [26] must be modified to accommodate the G factor and gives

$$r = \frac{I_{vv} - G \times I_{vh}}{I_{vv} + 2G \times I_{vh}}. \quad [28]$$

Most commercially available instruments have an option for correcting the single-point polarization measurements with the G factor, and it is very important to perform such corrections carefully.

Polarization artifacts in emission measurements. When a ligand binding experiment is performed by collecting fluorescence intensity, the polarization throughout the titration is assumed to be constant. If, on the other hand, the polarization of the emission changes with binding, then a correction must be made to the emission intensities, or spectra, that are collected. Because of the instrument polarization bias, polarization changes in the sample will lead to erroneous intensities, which will be weighted by the polarization, as well as by the fraction bound.

In a standard fluorometer, the sample emission is measured at right angles to the excitation path, as mentioned above. It can be easily shown that in this geometry, and with the excitation light polarized vertically, the total emission intensity is proportional to $I_{total} = I_{vv} + 2I_{vh}$ (56, 79). Emission corrections can be made by independently collecting the intensity components (or spectra) and calculating the corrected total intensity. A simpler and more routine approach is to set the fluorometer polarizers to the magic angle conditions with the excitation polarizer set to 0° (vertical) and the emission polarizer set to 54.7° (56). This condition will essentially provide a twofold increase in $I_\perp$ over $I_\parallel$ to yield corrected I_{total} at any wavelength. An alternative experimental setup for magic angle conditions entails setting the excitation polarizer to 35° while monitoring the emission without a polarizer. The latter setup is recommended when sample emission intensities are weak and the instrument sensitivity needs to be maximized.

Inner filter effect. The inner filter effect is the reduction of the fluorescence of a given sample due to the absorption of the excitation light and the absorption of the light emitted by the sample itself. To minimize this artifact, the total sample absorption (antibody and hapten) should be kept low, less than 0.05 OD at the excitation and emission wavelengths. If the sample absorption at either wavelength becomes large, then one can use short-path-length cuvettes to reduce the absorption or attempt to correct the fluorescence intensity by using the formula (56)

$$I_{corr} \cong I_{em}\ \text{antilog}\left(\frac{OD_{ex} + OD_{em}}{2}\right). \quad [29]$$

Equation [29] is approximate only. For precise corrections it is essential to obtain a calibration plot (fluores-

cence intensity at emission wavelength vs optical density at excitation wavelength) for a given fluorometer because the collection optics also play a role in the impact of the inner filter effect.

ACKNOWLEDGMENTS

We thank Enrico Gratton (University of Illinois, Urbana) for helpful discussions, William Mantulin (University of Illinois, Urbana) and David Jameson (University of Hawaii, Honolulu) for advice on manuscript preparation, Edmund Matayoshi (Abbott Labs) for comments on FCS, and Philip Carrigan (Abbott Labs) for critical reading of the manuscript. S.Y.T. expresses special thanks to Darlene Cotter and Jose Pagan (Abbott Labs) for their interest and support. T.L.H. is supported by the National Institutes of Health (RR03155).

REFERENCES

1. Padlan, E. A. (1996) *Adv. Prot. Chem.* **49,** 57–133.
2. Landsteiner (1962) The Specificity of Serological Reactions, Dover, New York.
3. Klotz, I. M. (1946) *Arch. Biochem.* **9,** 109–117.
4. Scatchard, G. (1949) *Ann. N.Y. Acad. Sci.* **51,** 660–672.
5. Klotz, I. M. (1985) *Q. Rev. Biophys.* **18,** 227–259.
6. Weber, G., and Anderson, S. (1965) *Biochemistry* **4,** 1942–1947.
7. Johnson, M. L. (1992) *in* Methods in Enzymology: Numerical Computer Methods (Brand, L., and Johnson, M., Eds.), Vol. 210, pp. 68–87, Academic Press, New York.
8. Weber, G. (1992) Protein Interactions, Routledge, Chapman, & Hall, New York.
9. Winzor, D. J., and Sawyer, W. H. (1995) Quantitative Characterization of Ligand Binding, Wiley–Liss, New York.
10. Eftink, M. R. (1997) *in* Methods in Enzymology: Fluorescence Spectroscopy (Brand, L., and Johnson, M. L., Eds.), Vol. 278, pp. 221–257, Academic Press, New York.
11. Tetin, S. Y., Rumbley, C. A., Hazlett, T. L., and Voss, E. W. J. (1993) *Biochemistry* **32,** 9011–9017.
12. Adair, G. S. (1925) *J. Biol. Chem.* **63,** 529–545.
13. Cantor, C. R., and Schimmel, P. R. (1980) Biophysical Chemistry, Part III: The Behavior of Biological Macromolecules, Freeman, San Francisco.
14. Klotz, I. M. (1986) Introduction to Biomolecular Energetics, Academic Press, New York.
15. Klotz, I. M., and Hunston, D. L. (1984) *J. Biol. Chem.* **259,** 10060–10062.
16. Royer, C. A., Smith, W. R., and Beechem, J. M. (1990) *Anal. Biochem.* **191,** 287–294.
17. Taylor, J. R. (1982) An Introduction to Error Analysis, University Science Books, Mill Valley, CA.
18. Weber, G. (1965) *in* Molecular Biophysics (Pullman, B., and WeissBluth, M., Eds.), pp. 369–397, Academic Press, New York.
19. Wang, C.-H. J., Stroupe, S. D., and Jolley, M. E. (1987) U.S. Patent 4,668,640.
20. Di Cera, E. (1992) *in* Methods in Enzymology: Numerical Computer Methods (Brand, L., and Johnson, M., Eds.), Vol. 210, pp. 68–87, Academic Press.
21. Kranz, D. M., and Voss, E. W., Jr. (1981) *Mol. Immunol.* **18,** 889–898.
22. Herron, J. N., He, X., Mason, M. L., Voss, E. W., and Edmundson, A. B. (1989) *Proteins* **5,** 271–280.
23. Droupadi, P. R., Mayers, E. A., and Linthicum, D. S. (1994) *J. Protein Chem.* **13,** 297–306.
24. Anchin, J. M., Droupadi, P. R., DuBois, G. E., Kellogg, M. S., Nagarajan, S., Carter, J. S., and Linthicum, D. S. (1994) *J. Immunol.* **153,** 3059–3069.
25. Gudgin-Templeton, E. F., and Ware, W. R. (1985) *Mol. Immunol.* **22,** 45–55.
26. Arbeloa, L., and Ojeda, P. R. (1982) *Chem. Phys. Let.* **87,** 556–560.
27. Winder, A. F., and Gent, W. L. (1971) *Biopolymers* **10,** 1243–1251.
28. Toptygin, D., and Brand, L. (1995) *Anal. Biochem.* **224,** 330–338.
29. Athey, T. W., and Cathou, R. E. (1977) *Immunochemistry* **14,** 397–404.
30. Tetin, S. Y., Mantulin, W. W., Denzin, L. K., Weidner, K. M., and Voss, E. W., Jr. (1992) *Biochemistry* **31,** 12029–12034.
31. Strickland, E. H. (1974) *CRC Crit. Rev. Biochem.* **2,** 113–175.
32. Grishina, I. B., and Woody, R. W. (1994) *Faraday Discuss.* **99,** 245–262.
33. Tetin, S. Y., and Linthicum, D. S. (1995) *Biochemistry* **35,** 1258–1264.
34. Weber, G., and Teale, F. W. J. (1957) *Trans. Faraday Soc.* **53,** 646–648.
35. Weber, G. (1960) *Biochem. J.* **75,** 335–345.
36. Callis, P. R. (1997) *Methods Enzymol.* **278,** 113–150.
37. Herron, J. N., Terry, A. H., Johnston, S., He, X., Guddat, L. W., Voss, E. W., and Edmundson, A. B. (1994) *Biophys. J.* **67,** 2167–2183.
38. Guddat, L., Shan, L., Anchin, J., Linthicum, D. S., and Edmundson, A. B. (1994) *J. Mol. Biol.* **236,** 247–274.
39. Velick, S. F., Parker, C. W., and Eisen, H. N. (1960) *Proc. Natl. Acad. Sci. USA* **46,** 1470–1482.
40. Eisen, H. N., and Siskind, G. W. (1964) *Biochemistry* **3,** 996–1008.
41. French, D. L., Laskov, R., and Scharff, M. D. (1989) *Science* **244,** 1152–1157.
42. Kocks, C., and Rajewsky, K. (1989) *Annu. Rev. Immunol.* **7,** 537–559.
43. Viswanathan, M., Pledger, D. W., Tetin, S. Y., Linthicum, D. S., and Subramaniam, S. (1996) *Biopolymers* **39,** 395–406.
44. Smith, R. G., Ballard, D. W., Blier, P. R., Pace, P. E., Bothwell, A., Herron, J. N., Edmundson, A. B., and Voss, E. W. (1989) *J. Indian Inst. Sci.* **69,** 25–46.
45. Herron, J. N., He, X.-M., Gibson, A. L., Ballard, D. W., Blier, P., Pace, P., Bothwell, A., Voss, E. W., and Edmundson, A. B. (1991) *Proteins* **11,** 159–175.
46. Rumbley, C. A., Denzin, L. K., Yantz, L., Tetin, S. Y., and Voss, E. W., Jr. (1993) *J. Biol. Chem.* **268,** 13667–13674.
47. Cowgill, R. W. (1970) *Biochim. Biophys. Acta* **207,** 556–559.
48. Chen, Y., and Barkley, M. D. (1998) *Biochemistry* **37,** 9976–9982.
49. Harris, D. L., and Hudson, B. S. (1990) *Biochemistry* **29,** 5276–5285.
50. Harris, D. L., and Hudson, B. S. (1991) *Chem. Phys.* **158,** 353–582.
51. Eftink, M. R. (1991) *in* Topics in Fluorescence Spectroscopy (Lakowicz, J. R., Ed.), Vol. 2, pp. 53–120, Plenum Press, New York/London.

52. Kranz, D. M., Herron, J. N., and Voss, E. W. (1982) *J. Biol. Chem.* **257,** 6987–6995.

53a. Weber, G. (1952) *Biochemistry* **51,** 145–155.

53b. Weber, G. (1952) *Biochemistry* **51,** 155–167.

54. Perrin, F. (1926) *J. Phys. Radium* **7,** 390–401.

55. Jablonski, A. (1960) *Bull. Acad. Pol. Sci.* **8,** 259–264.

56. Lakowicz, J. R. (1983) Principles of Fluorescence Spectroscopy, Plenum Press, New York/London.

57. Zagyansky, Y. A., Nezlin, R., and Tumerman, L. A. (1969) *Immunochemistry* **6,** 787–800.

58. Yguerabide, J., Epstein, H. F., and Stryer, L. (1970) *J. Mol. Biol.* **51,** 573–590.

59. Magde, D., Elson, E. L., and Webb, W. W. (1972) *Phys. Rev. Lett.* **29,** 705–711.

60. Magde, D., Elson, E. L., and Webb, W. W. (1974) *Biopolymers* **13,** 29–61.

61. Elson, E. L., and Magde, D. (1974) *Biopolymers* **13,** 1–27.

62. Eigen, M., and Rigler, R. (1994) *Proc. Natl. Acad. Sci. USA* **91,** 5740–5747.

63. Rigler, R., Windengren, J., and Mets, U. (1992) Fluorescence Spectroscopy New Methods and Applications, pp. 13–24, Springer Verlag, New York.

64. Rigler, R. (1995) *J. Biotech.* **41,** 177–186.

65. Koppel, D. E., Axelrod, D., Schlessinger, J., Elson, E. L., and Webb, W. W. (1976) *Biophys. J.* **16,** 1315–1329.

66. Qian, H., and L., E. E. (1988) *SPIE* **909,** 352–359.

67. Qian, H., and L., E. E. (1991) *Appl. Opt.* **30,** 1185–1195.

68. Berland, K. M., So, P. T., and Gratton, E. (1995) *Biophys. J.* **68,** 694–701.

69. Svedberg, T., and Inouye, K. (1911) *Z. Phys. Chem.* **77,** 145–191.

70. von Smoluchowski, M. (1914) *Wien Berichte.* **123,** 2381.

71. Tetin, S. Y., Swift, K. M., and Matayoshi, E. D. (1998) *in* Abstracts, 25th FEBS Meeting, p. 7.36, Copenhagen.

72. Tetin, S. Y., Swift, K. M., and Matayoshi, E. D. (1999) In preparation.

73. Palmer, A. G., and Thompson, N. L. (1987) *Biophys. J.* **52,** 257–270.

74. Chen, Y., Müller, J. D., Carlson, K. A., Katzenellenbogen, J. A., and Gratton, E. (1998) *Biophys. J.* **74,** A182.

75. Chen, Y., Müller, J. D., Eid, J., Tetin, S. Y., and Gratton, E. (1999) *Biophys. J.* **76,** A445.

76. Schwille, P., Meyer-Almes, F. J., and Rigler, R. (1997) *Biophys. J.* **72,** 1878–1886.

77. Koltermann, A., Kettling, U., Bieschke, J., Winkler, T., and Eigen, M. (1998) *Proc. Natl. Acad. Sci. USA* **95,** 1421–1426.

78. Kettling, U., Koltermann, A., Schwille, P., and Eigen, M. (1998) *Proc. Natl. Acad. Sci. USA* **95,** 1416–1420.

79. Jameson, D. M., and Hazlett, T. L. (1991) *in* Biophysical and Biochemical Aspects of Fluorescence Spectroscopy (Dewey, G., Ed.), pp. 105–133, Plenum Press, New York.